Published in final edited form as:
Int J Comput Assist Radiol Surg. 2012 March ; 7(2): 181–190. doi:10.1007/s11548-011-0598-9.

Robotic system for MRI-guided prostate biopsy: feasibility of teleoperated needle insertion and ex vivo phantom study

Reza Seifabadi
Laboratory for Computational Sensing and Robotics (LCSR), The Johns Hopkins University, Baltimore, MD, USA

Laboratory for Percutaneous surgery (Perk Lab), Queen's University, Kingston, ON, Canada

Sang-Eun Song
Department of Radiology, Brigham and Women's Hospital and Harvard Medical School, Boston, MA, USA

Axel Krieger
Laboratory for Computational Sensing and Robotics (LCSR), The Johns Hopkins University, Baltimore, MD, USA

Nathan Bongjoon Cho
Laboratory for Computational Sensing and Robotics (LCSR), The Johns Hopkins University, Baltimore, MD, USA

Junichi Tokuda
Department of Radiology, Brigham and Women's Hospital and Harvard Medical School, Boston, MA, USA

Gabor Fichtinger
Laboratory for Computational Sensing and Robotics (LCSR), The Johns Hopkins University, Baltimore, MD, USA

Laboratory for Percutaneous surgery (Perk Lab), Queen's University, Kingston, ON, Canada

Iulian Iordachita
Laboratory for Computational Sensing and Robotics (LCSR), The Johns Hopkins University, Baltimore, MD, USA

Abstract

Purpose—Magnetic Resonance Imaging (MRI) combined with robotic assistance has the potential to improve on clinical outcomes of biopsy and local treatment of prostate cancer.

Methods—We report the workspace optimization and phantom evaluation of a five Degree of Freedom (DOF) parallel pneumatically actuated modular robot for MRI-guided prostate biopsy. To shorten procedure time and consequently increase patient comfort and system accuracy, a prototype of a MRI-compatible master–slave needle driver module using piezo motors was also added to the base robot.

Results—Variable size workspace was achieved using appropriate link length, compared with the previous design. The 5-DOF targeting accuracy demonstrated an average error of 2.5mm

reza.seifabadi@queensu.ca.

Conflict of interest None.

(STD=1.37mm) in a realistic phantom inside a 3T magnet with a bevel-tip 18G needle. The average position tracking error of the master–slave needle driver was always below 0.1mm.

Conclusion—Phantom experiments showed sufficient accuracy for manual prostate biopsy. Also, the implementation of teleoperated needle insertion was feasible and accurate. These two together suggest the feasibility of accurate fully actuated needle placement into prostate while keeping the clinician supervision over the task.

Keywords

Transperineal prostate biopsy; MRI compatible; Pneumatic robot; Teleoperation; Accuracy evaluation; Phantom study

Introduction

Prostate cancer is the most common cancer in men in the United States. In 2010, over 200,000 men were expected to be diagnosed with prostate cancer with over 32,000 deaths of this disease [1]. Early stage cancer detection is critically important to ensure patient survival. Despite its poor specificity, PSA level is used to determine which patient is a candidate for core needle biopsy. Each year approximately 1.5 million prostate biopsy procedures are performed only in the United States [2]. For this reason, a surgical biopsy needle is inserted into a predefined target position inside prostate under image guidance.

Transrectal ultrasound (TRUS) guidance is the “Gold Standard” navigation method for the biopsy due to its real-time nature, relative low cost, and ease of use. However, this imaging modality is not capable of visualizing cancer [3] but rather the contour of prostate, resulting in a significant number of false negatives in conventional TRUS-guided systematic biopsy, where 6–12 cores equally distributed within the prostate are sampled.

MRI is a superior imaging modality, primarily due to its high sensitivity for detecting prostate tumors, excellent soft tissue contrast, high spatial resolution, and multi-planar volumetric imaging capabilities [4]. Despite its unique capabilities, MRI has two main limitations when it comes to a robotic approach: strong magnetic field (1.5T or greater) that requires MRI compatibility of surgical devices, sensors, and actuators as well as physical limitation of in-bore access and workspace.

Several MRI-compatible robots have been reported for prostate intervention. The robotic systems can be categorized into transrectal, transperineal, and transgluteal depending upon the anatomical access method used [8].

(1) *Transrectal approach*: In [5–7] two generations of MRI-guided systems were developed for transrectal prostate biopsies, therapeutic injections, and marker placements. APT I had 2-DOF (roll and pitch) and was actuated manually through two flexible shafts coming out of the bore. APT II has been used in many clinical procedures at a few health care institutions. In [8], a motorized APT is introduced where the roll and pitch movements are actuated using piezo motors. In [9] Beyersdorff and in [10], Engelhard developed MRI-guided transrectal needle biopsies in patient studies with a system (Invivo Germany GmbH, Schwerin, Germany) employing manual alignment of a needle sleeve. Elhawary reported a prototype robotic system using linear piezo-ceramic motors for transrectal prostate biopsy [11]. This system employed remotely driven needle driver module with haptic force feedback at the master side.

(2) *Transperineal approach*: MRI-guided transperineal prostate intervention was primarily studied in patient experiment inside an open MRI scanner [12] and

then conventional closed MRI scanner [13]. In [14] and [15], Chinzei and Di Maio designed systems to assist transperineal intra-prostatic needle placement. In [16], Tadakuma developed an MRI-compatible robot for transperineal needle placement in the prostate using dielectric elastomer actuators (DEAs). In [17], Stoianovici developed a fully automated pneumatically actuated device for transperineal brachytherapy seed placement in phantom experiment. In [18], Fischer developed a pneumatic 2-DOF robot for transperineal prostate needle placement in phantom study. In [19], Goldenberg developed a robotic system employing ultrasonic actuators for MRI-guided transperineal prostate intervention. In [20], van den Bosch reported a hydraulically and pneumatically actuated tapping device to alleviate undesirable prostate displacement and deformation. Su reported a 3-DOF Cartesian robot for MRI-guided transperineal needle alignment with a 3-DOF needle steering module for teleoperated and autonomous seed implantation [21,22].

(3) *Transglutteal approach*: In [23], Zangos proposed and clinically validated the feasibility of manual transgluteal approach with an open 0.2T MRI scanner. In [24], Zangos used the Innomotion robot for transgluteal approach in a cadaver study at 1.5T.

With the use of low-friction MRI-compatible pneumatic actuators, we have developed a high-field 3T MRI-guided prostate intervention system for transperineal needle placement procedures. Figure 1 shows the latest robot prototype that provides 4-DOF surgical needle alignment in MRI coordinate with a platform for the manual needle insertion as the 5-th DOF. The previous reports focused on pneumatic actuator control, workspace design and targeting functions [25], signal-to-noise ratio (SNR) test for MRI compatibility [26], and overall system integration and procedural description [27]. In this study, we report the latest workspace optimization of the robot and the 5-DOF targeting accuracy assessment in phantom experiment. Also, the robot sterilization is addressed.

Although this robot is able to align the surgical needle toward a predefined target inside prostate, the needle needs to be inserted manually. For this reason, the patient has to be pulled out of the bore twice each biopsy, i.e. once for manual insertion and once for tissue removal after taking confirmation image. In order to shorten the procedure time, we have proposed adding a teleoperated needle driver module on the robot which can eliminate the first move-out if a remote triggering mechanism is implemented as well. This needle driver is a separate MRI-compatible module driven remotely by a master device placed outside the bore. In this way, the procedure time can be notably shortened providing patient comfort, which subsequently reduces unwanted target movement caused by patient motion. For the same reason, it may reduce the necessity of confirmation imaging, as well.

Several teleoperated needle placement systems under MRI guidance have been investigated. In [28], Kokes reports a teleoperated hydraulic needle driver robot with haptic feedback for Radio Frequency Ablation (RFA) of breast tumors under continuous MRI guidance. In [29], Su reports a 3-DOF teleoperated needle driver installed on top of a 3-DOF Cartesian linear stage for brachytherapy. In [30], Tse reports a 5-DOF robot for needle alignment with a single DOF teleoperated module for transrectal prostate biopsy.

Unlike previously discussed systems, our master device is designed to be placed inside scanner room as surgeons need to be close to the patient during the interventional procedure. This means that conventional (non-MRI compatible) haptic devices cannot be deployed due to the high magnetic field. This paper reports the initial study of a human-controlled needle drive added to an existing robot.

The paper is organized as follows: system architecture and procedure are discussed in “System design”. In “Needle driver module design”, teleoperated needle driver module is introduced and discussed. Workspace optimization is briefly discussed, as well. In “Experiments and results”, the overall system needle placement accuracy is evaluated in phantom experiment inside a 3T magnet. Also, the performance of the proposed teleoperated needle insertion driver is evaluated. The paper is continued by discussion in “Discussion” and ends by conclusions and future works in “Conclusions and future works”.

System design

System components

Figure 2 illustrates a diagram of system components and information flow. In MRI suite (left side), the patient and the robot are placed inside scanner and the robot controller is placed at 3 m distance from the scanner's bore. The medical air supply available in a standard hospital is used to run the pneumatic robot. The controller sends the pressure signals (commands) to the robot pneumatic actuators and receives position feedback from the robot optical encoders. There is no electrical communication between them in order to keep the Electro Magnetic Interference (EMI) minimized. The power supply for the controller is placed in the control room to further reduce the EMI. In the control room (right side), the scanner console that is a workstation for running the MRI machine is placed. 3D Slicer (http://www.slicer.org/) is running on a Linux-based workstation called planning workstation. Intra-operative MRI images are imported from the scanner console to 3D Slicer. Target positions are selected by the clinician in this software and sent as commands to the robot controller. A local network is established among the planning workstation, the scanner console, and the robot controller. Data communication between the network and robot controller is via fiber-optic Ethernet to avoid EMI.

Dotted-line squares show new added components to the existing system as discussed earlier. These components include the following: the master console, the slave (needle driver module), and the master–slave control units. Currently, the needle driver controller is not integrated with the robot controller. The surgeon stands next to the scanner and moves the master console while observing the real-time image. The slave follows the master's movement and then performs insertion.

To avoid interference with the pubic arch and urethra, a 5-DOF parallel kinematic structure was proposed [25]. The pyramid structure of the robot helps to maximize the use of `under-legs' space and minimize `between-legs' space. If necessary, the workspace can be shifted vertically by inserting a spacer. Timing belts and pulleys transmit each pneumatic cylinder movement to the prismatic manipulation of front and rear triangle structures. These pulleys and timing belts function as external damping mechanism as well to stabilize cylinder's dynamic behavior and solve many of the difficulties associated with servo control of pneumatics. MRI-compatible optical encoders are used for position sensing. The moving parts are made of Ultem, which is sufficiently rigid and MRI compatible. The needle is located on the linkage connecting the front and back mechanisms.

The controller operates inside the scanner room, approximately 3 m away from the 3T scanner, without functional difficulties or significant image quality degradation [18]. The controller is inside an EMI-shielded enclosure contains the embedded Linux PC providing low-level servo control, the piezoelectric valves, pressure sensors, and the fiber-optic Ethernet converter. A customized graphical user interface (GUI) specifically designed for the prostate intervention is used with the robot [34].

In case of robot failure, the robot is removed and the procedure is continued manually by a grid of template similar to standard ultrasound-guided procedure [35,36].

Robot kinematics

The robot comprises two identical planar mechanisms (front and rear triangles) as shown in Fig. 3. Each planar parallel structure can move its end effector within the corresponding plane with the use of two pneumatic actuators 1 and 2 (3 and 4). As these two mechanisms are coupled together with an adjustable link and two spherical joints at both ends, they generate yaw and pitch orientations as well as x and y in-plane movement if moved asynchronous, resulting in 4-DOF. The 5th DOF, i.e. the insertion, is performed manually. Each 2-DOF mechanism provides a workspace surrounding a sphere of 50mm diameter (Fig. 3b).

The way the robot reaches a target (i.e. the inverse kinematics) is as follows: first, a target and a straight trajectory (considering pubic arc/urethra avoidance) are specified by clinician in the navigation software. These target and trajectory are given in MRI coordinate system and thus needed to be transformed into robot coordinate system. For this reason, Z-frame is used [37]. Then, the line defined by the target and the trajectory intersects the front and rear planes (Fig. 3a) giving (x_1, y_1) and (x_2, y_2). Then, each 2-DOF planar mechanism must move as follows such that the effectors reach those coordinates (Fig. 3b):

$$J_1 = x_1 + \sqrt{\left(L^2 - (y_1 - a)^2\right)},\ J_2 = x_1 - \sqrt{\left(L^2 - (y_1 - a)^2\right)}$$

where J_1 and J_2 are x coordinates of each actuator. Similar relationship exists for J_3 and J_4 (back triangle mechanisms) with replacing x_2 and y_2 for x_1 and y_1.

Workspace optimization

The robot was designed with variable link length so that robot's workspace can easily be modified or intra-operatively changed depending upon the prostate size and height relative to the table. Considering the robot kinematics (Fig. 3a), the rear triangle requires larger manipulation range because the front triangle is fundamentally responsible for needle entry area and the rear triangle is responsible for angulations. Also, since insertion angle is usually upwards i.e. posterior-to-anterior, shorter rear triangle link length would benefit. Originally, 120mm link length was designed for all triangle links. However, 120/100mm for front triangle link and 120/100/80mm for rear triangle are currently available. Figure 4 shows an axial view of 120mm front—120mm rear workspace (a) and 120mm front—80mm rear workspace (b). As seen, the 2D workspace has enlarged as the result of shortening the back links.

Sterilization

Prostate biopsies that are performed through the rectum do not require sterilization. In contrast, we propose a system for transperineal access that requires some degree of sterilization. Compared with the conventional prostate biopsy system in which a disposable grid template is used, the brass tube in front triangle which guides the needle through (Fig. 8) is not disposable and rather permanently attached to the links by the front spherical joint. Hence, for the current version, we proposed to dismantle the top parts (Fig. 8, dotted-line area) as an ensemble and send to the plasma sterilization before each procedure. The non-sterile parts are covered by a plastic drape with a small hole for the needle to travel through (Fig. 5). The use of drape did not show interference with the robot's movement.

Needle driver module design

The clinical workflow of this robotic system is as follows:

(1) Patient is placed inside the bore;

(2) Z-frame is placed on a predefined position on the custom-made MRI board;

(3) Z-frame is scanned and 3D Slicer find the transformation matrix from MRI coordinate to robot coordinate;

(4) Z-frame is removed;

(5) Robot is placed between patient's legs on a predefined position on custom-made MRI board;

(6) Intra-operative MRI image of the anatomy is acquired and imported in navigation software;

(7) One target and needle trajectory is specified in planning workstation;

(8) Planning software (3D Slicer) sends the transformation matrix and target information to the robot controller;

(9) The controller solves the Inverse Kinematic Problem (IKP) and commands the robot actuators to orient the needle toward the target;

(10) The patient is pulled out of the bore;

(11) The surgeon inserts the needle manually;

(12) Patient is placed back into MRI;

(13) Confirmation image is taken;

(14) The needle tip is compared with the planned target in axial plane and targeting error is found;

(15) If the error is acceptable (<3mm), patient is pulled out for tissue removal and go to next target starting from (7);

(16) Otherwise, patient is pulled out for needle removal and go to the same target starting from (7).

The important issue with the manual insertion is that the second move-out followed by move-in (underlined above) not only extends the procedure duration by itself but also raises the risk of targeting failure as the result of patient movement, thus causing repetition of items 7–15. Hence, this study aims to eliminate manual needle insertion so as to reduce the procedure time and boost patient comfort. Automated needle insertion is not the solution due to safety issue. The solution proposed here is a teleoperated needle insertion. As depicted in Fig. 6, the surgeon stands in MRI room, next to the patient and operates an MRI-compatible master device, which fairly mimics a realistic needle insertion. Also, the surgeon will be able to benefit from real-time MRI image through a screen inside the MRI room. In this way, surgeon will have a more realistic sense of doing the task.

The requirements for this teleoperatoin system can be summarized as follows:

(1) The needle driver should precisely follow the master position not only in free space movement, but also during the insertion (i.e. $q_1 = q_2$).

(2) The system should be MRI compatible with negligible SNR degradation.

(3) The needle driver should be sufficiently compact such that it can be mounted on top of the base robot.

(4) The slave must be sufficiently strong to penetrate the tissue (at least 8.9N [30]).

Needle driver (slave robot)

The needle driver is designed to be installed on top of the linkage between the front and the rear triangles. The needle driver is located close to the scanner's iso-center, and MRI compatibility becomes the first concern for actuator selection. Based upon the previous experience, pneumatic actuators are hard to control especially when they are configured as a master–slave system. This is due mainly to the air compressibility and their inherent non-linearity of the pneumatic actuator. An alternative to pneumatic actuator is piezo motor, which provides high precision and ease of control. Moreover, piezo motor generates enough force in a small footprint. We compared three different types of piezo motors: Nanomotion Ltd. (Yoqneam, Israel), PI PILine (Physik Instrumente, Karlsruhe, Germany) and Piezomotor Piezoleg (Piezomotor AB, Upsala, Sweden). Table 1 shows the comparison.

As a result, Nanomotion motor was selected as it provides not only enough thrust for penetrating prostate (almost 8.9N [30]) but also MRI compatibility.

In order to achieve the given clinical task, the module should:

- Provide sufficient thrust;
- Be sufficiently compact so that it can be installed on the top of the robot;
- Be MRI compatible (minimum image degradation);
- Be as frictionless as possible since mechanical friction obstructs the needle–tissue interaction.

To measure position, optical encoders are employed as follows: modular EM1 electro optical encoders (US Digital, Vancouver, Washington), along with a 500 lines per inch (LPI) code strip. Figure 7 shows a close-up view of stage using two Nanomotion HR-4 motors with four motor elements each (28N together). This stage was previously used as the linear stage for the motorized APT robot [8]. A low-cost, custom-made linear stage was built, because off-the-shelf linear bearings are usually not MRI compatible and costly. A pairs of HR-4 Nanomotion motors were axially pre-loaded against each other on a ceramic drive strips and provided linear motion of a drive shaft that slides axially forward and backward on an aluminum plate. Vertical and horizontal stops are used to limit vertical movement and define end stops for travel. All materials are non-metalic (Ultem, plastic, or ceramic) except the motor plate that was made of aluminum for increased rigidity. Figure 8 shows this module installed on top of the robot.

Master device

In our preliminary prototype (Fig. 9), the master device is not yet actuated. It consists of a MRI-compatible slide and rail (Igus Inc., East Providence, RI) which mimics the needle insertion. To measure position, optical encoding was employed with 500 lines per inch (LPI) code strip. In the next step, a linear module similar to the needle driver will replace the current master device, in order to generate haptic force feedback on surgeon's fingers.

Needle driver controller unit

The needle driver controller unit consists of Nanomotion AB5 motor amplifiers, a DMC-21×3 Ethernet motion controller (Galil Motion Control, Rocklin, California) (Fig. 10), and a PC workstation on which GalilTools (the software to command the controller and to

monitor sensor signals) runs. A 24V DC power supply is used to run the controller and amplifier. If shielded properly, the SNR degradation as the result of using AB5 amplifiers would be negligible as long as the motor is not moving (even if in the motor-on mode) [8]. However, in our application, the motor is running while the scanner is operating. This will impact the SNR noticeably. For this reason, we are planning to replace AB5 with a custom-made amplifier, which will eliminate the high-frequency switching of the current amplifier.

Experiments and results

Ex vivo accuracy evaluation with manual insertion

In the earlier studies, we evaluated the system in the following three series of preliminary experiments: (1) manipulator positioning accuracy and repeatability test [25], (2) signal-to-noise ratio (SNR) test for MRI compatibility [26], and (3) patient compatibility and comfort tests for system integration and procedural feasibility [27]. Here, we performed an ex vivo experiment (Fig. 1) using a commercial prostate intervention training phantom (Model 053 Ultrasound Prostate Training Phantom, Computerized Imaging Reference Systems, Inc., Norfolk, VA). The objective of this experiment was to evaluate the overall accuracy of needle placement in prostate biopsy procedures. The prostate phantom was placed and fixed in a height typical in a real clinical procedure. In the beginning, the Z-frame was secured on the predefined position on the custom-made MRI table. The image of the Z-frame was acquired using 3D Fast Low Angle Shot (FLASH) (TR/TE: 12/1.97ms; acquisition matrix: 256 × 256; flip angle 45°; field of view: 160 × 160 mm; slice thickness: 2mm; receiver bandwidth: 400 Hz/pixel; number of averages: 3). After imaging the Z-frame, the images were uploaded in 3D Slicer and the transformation matrix from RAS (Right/Left, Anterior/Posterior, Superior/Inferior) to robot coordinate (XYZ) was calculated by the software. The prostate phantom was then imaged and imported to the navigation software. The image of the phantom was acquired using 2D Turbo Spin Echo (TSE) sequence (TR/TE=5,250/100ms; acquisition matrix = 320 × 224; flip angle 150°; field of view = 140 × 140 mm; slice thickness=3mm; receiver bandwidth=203 Hz/pixel). Then, the Z-frame was removed, and the robot was placed in a certain pose on MRI board. In 3D Slicer, a total of 15 targets were randomly picked within the prostate capsule in the phantom, as indicated in Table 2. These targets were chosen in different area of the prostate capsule to ensure the reported average error is independent of the target location. The software sent those targets and corresponding needle trajectories (in quaternion format) to the robot controller along with the RAS-to-XYZ transformation matrix (calculated by Z-frame registration) via Ethernet cable. After a 18–gauge×20 cm needle with bevel-shaped tip (MRI Bio Gun, E-Z-EM, Westbury, NY) was inserted for each target, a confirmation image was acquired around the target with a Half Fourier Acquisition Single Shot Turbo Spin Echo (HASTE) sequence (TR/TE = 1000/102 ms; matrix = 320 × 179; flip angle = 150°; field of view = 280×224 mm; slice thickness=2mm; receiver bandwidth=780Hz/pixel) along axial and sagittal plane in order to measure the 2D needle placement error. The 2D needle placement error was defined as the distance between the predefined target and the center of the needle artifact on the same axial plane, as obtained. The error in S direction (normal to the axial image plane) was ignored as the needle artifact was visible in a slide before and after the predefined target. Moreover, the biopsy sample is typically 15–20mm implying that few millimeters of error in needle direction is practically insignificant. The error components in R and A direction (entitled Err_R and Err_A, respectively) as well as the overall in-plane error (entitled Err_Total) for each target are provided in Table 2. Figure 11 shows the histogram of the overall in-plane error for each target as well as the average error. Target 13 was an outlier, and it was eliminated. The results are discussed in “Discussion”.

Position tracking evaluation of the master–slave needle driver

The performance of the master–slave insertion module is explored separately as shown in Fig. 12. The main experimental objective of the needle driver system was to test whether the needle driver follows the command sent by the master device. A simple code was written in G-language (the language of GalilTools). The controller at the slave side was a Proportional-Integral (PI) controller with the KP=100 and KI=20. The master was moved back and forth over a 40mm range of motion for 20s, and it was expected that the slave follows the master without any delay. As seen, the needle driver was following the master accurately without noticeable delay. The average error was 0.03mm. This experiment was repeated 3 times, and the error was below 0.1mm in all cases.

Discussion

The required accuracy is determined by the clinically significant size of prostate cancer foci. Although there is no standard yet, it is generally agreed that 3mm accuracy is sufficient [38]. As seen in Fig. 11 and Table 2, the average of the overall system needle placement error (i.e. including the manipulator error and the registration error) for the manual insertion approach is 2.5mm (STD=1.37) which seems adequate. However, due to prostate motion in real clinical procedure, the clinical targeting error is expected to be somewhat larger [39].

As the master–slave needle insertion system is only replacing the manual insertion (i.e. the 5th DOF), it should not affect the 4-DOF robot targeting accuracy (i.e. the needle alignment). Also, Fig. 12 shows that the slave followed the master with high accuracy and with no noticeable time delay. Hence, the results of the two experiments together suggest that the proposed 5-DOF robotic system has acceptable accuracy.

Conclusions and future works

A transperineal pneumatic robot was developed for MRI-guided prostatic biopsy. The robot addressed problems associated with previously developed MRI-guided prostate robot systems, including workspace limitation, needle placement accuracy, sterilization, and MRI compatibility. Pre-patient mockup trial was carried out in order to investigate the overall system needle placement accuracy. As the latest development, a prototype of a needle driver module was introduced. This needle driver module was added on top of the robot and can run remotely by a master device placed close to scanner. In conclusion, the overall concept, design, and implementation showed feasibility in initial phantom experiments. Work continues toward a clinically certifiable implementation. Also, we are considering possible solutions for an MRI-compatible force measurement technology in order to feedback the insertion force to the clinician's hand. Studies have been carried out on MRI-compatible force sensors ([32] and the references therein) that are not commercially available and have various limitations. The only commercially available technology is FBG force sensors [33]. After implementing FBG force sensors, a tool will be given to the clinician so that they can distinguish between different stages of needle advancement.

Acknowledgments

This work was funded by the US National Institute of Health grants 5R01CA111288-04, 5R01EB002963-05, 5P01CA067165, and 5U41RR019703. Gabor Fichtinger was supported as Cancer Care Ontario Research Chair. We are grateful to Dr. Clare Tempany and Dr. Nobuhiko Hata (Department of Radiology, Brigham and Women's Hospital and Harvard Medical School, Boston MA, USA) for their support on the pre-clinical experiments.

References

1. American Cancer Society. Cancer facts and figures 2010. American Cancer Society; Atlanta: 2010.

2. Jemal, A.; Siegel, R.; Ward, E.; Hao, Y.; Xu, J.; Thun, MJ. Cancer Statistics, 2009. A Cancer Journal for Clinicians; CA: 2009. page caac.20006
3. Terris MK, Wallen EM, Stamey TA. Comparison of mid-lobe versus lateral systematic sextant biopsies in detection of prostate cancer. Urol Int. 1997; 59:239–242. [PubMed: 9444742]
4. Yu KK, Hricak H. Imaging prostate cancer. Radiol Clin North Am. 2000; 38(1):59–85. [PubMed: 10664667]
5. Chowning SL, Susil RC, Krieger A, Fichtinger G, Whitcomb LL, Atalar E. A preliminary analysis and model of prostate injection distributions. Prostate. 2006; 66(4):344–357. [PubMed: 16302267]
6. Krieger, A.; Metzger, G.; Fichtinger, G.; Atalar, E.; Whitcomb, LL. A hybrid method for 6-DOF tracking of MRI-compatible robotic interventional devices. Proceedings of the IEEE international conference on robotics and automation, vol 2006; Orlando, FL, USA. 2006. p. 3844-3849.
7. Krieger, A.; Susil, R.; Tanacs, A.; Fichtinger, G.; Whitcomb, L.; Atalar, E. A mri compatible device for MRI-guided transrectal prostate biopsy. International Society of Magnetic Resonance Imaging in Medicine, Tenth Scientific Meeting; Honolulu. 2002. p. 338
8. Krieger, A.; Iulian, I.; Sang-Eun, S.; Bongjoon, CN.; Peter, G.; Gabor, F.; Louis, W. Development and preliminary evaluation of an actuated MRI-compatible robotic device for MRI-guided prostate intervention. ICRA; AK, US: 2010.
9. Beyersdorff D, Winkel A, Hamm B, Lenk S, Loening SA, Taupitz M. MR imaging-guided prostate biopsy with a closed MR unit at 1.5T: Initial results. Radiology. 2005; 234(2):576–581. [PubMed: 15616117]
10. Engelhard K, Hollenbach HP, Kiefer B, Winkel A, Goeb K, Engehausen D. Prostate biopsy in the supine position in a standard 1.5- T scanner under real time MR-imaging control using a MR-compatible endorectal biopsy device. Eur Radiol. 2006; 16(6):1237–1243. [PubMed: 16447048]
11. Elhawary H, Zivanovic A, Rea M, Davies B, Besant C, McRobbie D, de Souza N, Young I, Lamprth M. The feasibility of MR image guided prostate biopsy using piezoceramic motors inside or near to the magnet isocentre. Int Conf Med Image Comput Comput Assist Interv. 2006; 9(Pt 1): 519–526.
12. D'Amico AV, Tempany CM, Cormack R, Hata N, Jinzaki M, Tuncali K, Weinstein M, Richie JP. Transperineal magnetic resonance image guided prostate biopsy. J Urol. 2000; 164(2):385–387. [PubMed: 10893591]
13. Susil R, Camphausen K, Choyke P, McVeigh E, GS GG, Ning H, Miller R, Atalar E, Coleman C, Menard C. System for prostate brachytherapy and biopsy in a standard 1.5T MRI scanner. Magn Reson Med. 2004; 52(3):683–687. [PubMed: 15334592]
14. Chinzei K, Hata N, Jolesz FA, Kikinis R. MRI-compatible surgical assist robot: system integration and preliminary feasibility study. Medical image computing and computer-assisted intervention (MICCAI). 2000; vol 1935:921–930.
15. DiMaio SP, Pieper S, Chinzei K, Hata N, Haker SJ, Kacher DF, Fichtinger G, Tempany CM, Kikinis R. Robot-assisted needle placement in open MRI: system architecture, integration and validation. Comput Aided Surg. 2007; 12(1):15–24. [PubMed: 17364655]
16. Tadakuma, K.; DeVita, LSY.; Dubowsky, S. The experimental study of a precision parallel manipulator with binary actuation: with application to MRI cancer treatment. Proceedings of the IEEE ICRA; Pasadena, USA. 2008.
17. Stoianovici D, Song D, Petrisor D, Ursu D, Mazilu D, Muntener M, Mutener M, Schar M, Patriciu A. MRI stealth robot for prostate interventions. Minim Invasive Ther Allied Technol. 2007; 16(4): 241–248. [PubMed: 17763098]
18. Fischer GS, Iordachita I, Csoma C, Tokuda J, DiMaio SP, Tempany CM, Hata N, Fichtinger G. MRI-compatible pneumatic robot for transperineal prostate needle placement. IEEE/ASME Trans Mechatron. 2008; 13(3):295–305.
19. Goldenberg AA, Trachtenberg J, Kucharczyk W, Yi Y, Haider M, Ma L, Weersink R, Raoufi C. Robotic system for closed bore MRI-guided prostatic interventions. IEEE/ASME Trans Mechatron. 2008; 13(3):374–379.
20. van den Bosch MR, Moman MR, van Vulpen M, Battermann JJ, Duiveman E, van Schelven LJ, de Leeuw H, Lagendijk JJW, Moerland MA. Mri-guided robotic system for transperineal prostate interventions: proof of principle. Phys Med Biol. 2010; 55(5):N133–N140. [PubMed: 20145293]

21. Su, H.; Harrington, K.; Cole, G.; Fischer, G. Modular needle steering driver for MRI-guided transperineal prostate intervention. IEEE ICRA, Workshop on snakes, worms and catheters; Anchorage, AK. 2010.
22. Su, H.; Zervas, M.; Cole, G.; Furlong, C.; Fischer, G. Real-time MRI-guided needle placement robot with integrated fiber optic force sensing. Proceedings of the IEEE international conference on robotics and automation (ICRA); China. 2011.
23. Zangos S, Eichler K, Engelmann K, Ahmed M, Dettmer S, Herzog C, Pegios W, Wetter A, Lehnert T, Mack MG, Vogl TJ. MRguided transgluteal biopsies with an open low-field system in patients with clinically suspected prostate cancer: technique and preliminary results. Eur Radiol. 2005; 15(1):174–182. [PubMed: 15351902]
24. Zangos S, Herzog C, Eichler K, Hammerstingl R, Lukoschek A, Guthmann S, Gutmann B, Schoepf UJ, Costello P, Vogl TJ. MR-compatible assistance system for punction in a high-field system: device and feasibility transgluteal biopsies of the prostate gland. Euro Radiol. 2007; 17(4): 1118–1124.
25. Song, S.; Cho, N.; Ficsher, G.; Hata, N.; Tempany, C.; Fichtinger, G.; Iordachita, I. Development of a pneumatic robot for MRI-guided transperineal prostate biopsy and brachytherapy: new approaches. Proceedings of the IEEE international conference on robotics and automation; Anchorage, USA. 2010.
26. Song, S.; Cho, N.; Tokuda, J.; Hata, N.; Tempany, C.; Fichtinger, G.; Iordachita, I. Computer-assisted radiology and surgery (CARS). Geneva, Switzerland: 2010. MRI compatibility study of a pneumatically actuated robotic system for transperineal prostate needle placement.
27. Song, S.; Cho, N.; Tokuda, J.; Hata, N.; Tempany, C.; Fichtinger, G.; Iordachita, I. Preliminary evaluation of a MRI-compatible modular robotic system for MRI-guided prostate interventions. BioRob, Tokyo, Japan: 2010.
28. Kokes R, Lister K, Gullapalli R, Zhang B, MacMillan A, Richard H, Desai JP. Towards a teleoperated needle driver robot with haptic feedback for RFA of breast tumors under continuous MRI. Med Image Anal. 2009; 13:445–455. [PubMed: 19303805]
29. Su, H.; Shang, W.; Cole, G.; Harrington, K.; Fischer, G. Haptic system design for MRI-guided needle based prostate brachytherapy. Haptic symposium; 2010.
30. Tse ZH, Elhawary H, Rea M, Young I, Davis BL, Lamperth M. A haptic unit designed for magnetic resonance guided biopsy. IMechE. 2009; 223:159–172.
31. Mewes, P.; Tokuda, J.; DiMaio, SP.; Fischer, GS.; Csoma, C.; Gobi, DG.; Tempany, C.; Fichtinger, G.; Hata, N. An integrated MRI and robot control software system for an MR-compatible robot in prostate intervention. Proceedings of the IEEE international conference on robotics and automation (ICRA); 2008.
32. Su, H.; Fischer, G. A 3-axis optical force/torque sensor for prostate needle placement in magnetic resonance imaging environments. Proceedings of the 2nd annual IEEE international conference on technologies for practical robot applications; Boston, MA, USA. 2009. p. 5-9.
33. Park, Y-L.; Elayaperumal, S.; Daniel, BL.; Kaye, E.; Pauly, KB.; Black, RJ.; Cutkosky, MR. MRI-compatible haptics: feasibility of using optical fiber Bragg grating strain-sensors to detect deflection of needles in an MRI environment; Toronto, Canada. International Society for Magnetic Resonance in Medicine (ISMRM); 2008. 2008
34. Tokuda J, Fischer GS, Papademetris X, Yaniv Z, Ibanez L, Cheng P, Liu H, Blevins J, Arata J, Golby AJ, Kapur T, Pieper S, Burdette EC, Fichtinger G, Tempany CM, Hata N. OpenIGTLink: an open network protocol for image-guided therapy environment. Int J Med Robotics Comput Assist Surg. 2009; 5(4):423–434.
35. Tuncali, K.; Tokuda, J.; Iordachita, I.; Song, SE.; Fedorov, A.; Oguro, S.; Lasso, A.; Fennessy, FM.; Tang, Y.; Tempany, CM.; Hata, N. 3T MRI-guided transperineal trgeted prostate biopsy: clinical feasibility, safety, and early results. ISMRM; 2011.
36. Tokuda, J.; Tuncali, K.; Iordachita, I.; Song, SE.; Fedorov, A.; Oguro, S.; Lasso, A.; Fennessy, FM.; Tang, Y.; Tempany, CM.; Hata, N. Preliminary accuracy evaluation of 3T MRI-guided transperineal prostate biopsy with grid template. ISMRM; 2011.

37. Masamune K, Fichtinger G, Patriciu A, Sakuma I, Dohi T, Stoianovici D. System for robotically assisted percutaneous procedures with computed tomography guidance. J Comp Aided Surg. 2001; 6:370–383.

38. Van der Kwasta TH, Woltersc T, Evansa A, Roobolc M. Single prostatic cancer foci on prostate biopsy. Eur Urol Suppl. 2008; 7(8):549–556.

39. Xu, H.; Lasso, A.; Vikal, S.; Guion, P.; Krieger, A.; Kaushal, A.; Whitcomb, LL.; Fichtinger, G. MRI-guided robotic prostate biopsy: a clinical accuracy validation. Medical image computing and computer-assisted intervention (MICCAI); 2010. p. 383-391.

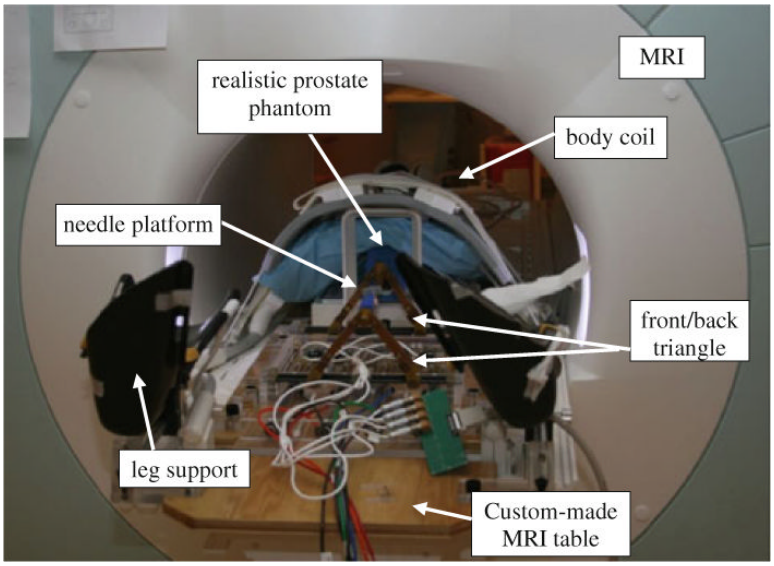

Fig. 1.
Latest prototype of the pneumatically actuated 5-DOF robot for MRI-guided transperineal prostate needle placement: realistic phantom experiment inside 3T magnet

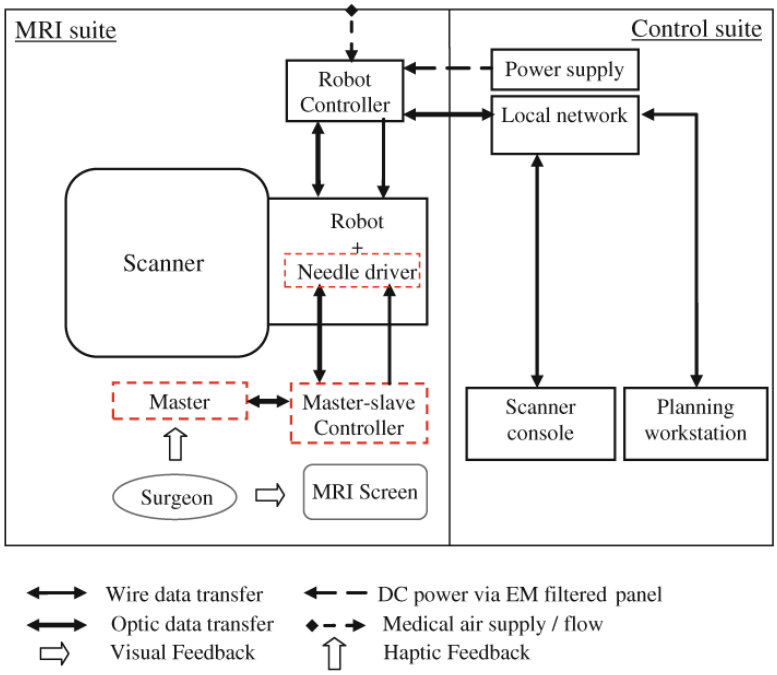

Fig. 2.

Diagram of system components and information flow. *Dotted-line squares* show new added components to the previous setup

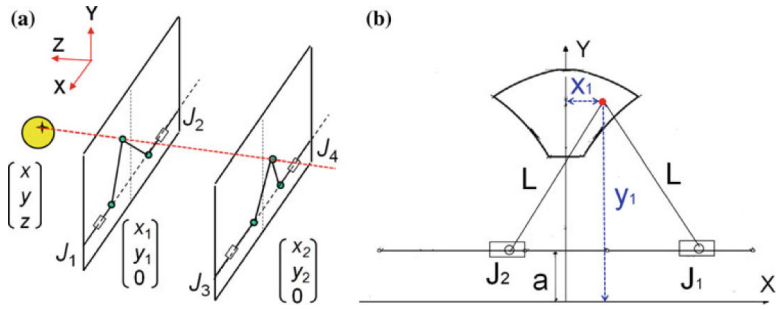

Fig. 3.

The manipulator consists of a pair of identical 2-DOF planar mechanism (**a**). Planar mechanism workspace and in-plane inverse kinematics relationship are shown (**b**)

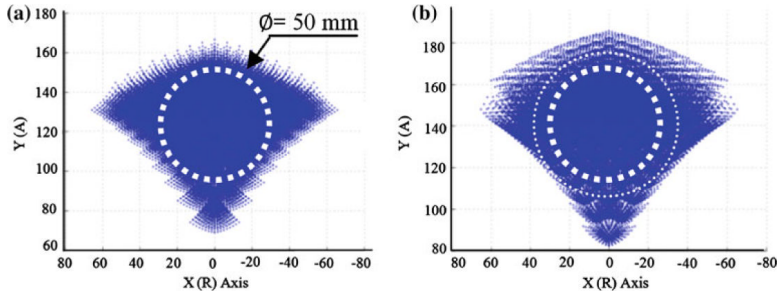

Fig. 4.

2D view of robot workspace when front/rear triangles link length are changed: **a** 120/120: a sphere of 50 mm diameter represents a relatively large prostate, **b** 120/80: The 2D workspace is enlarged as the result of shortening the back links

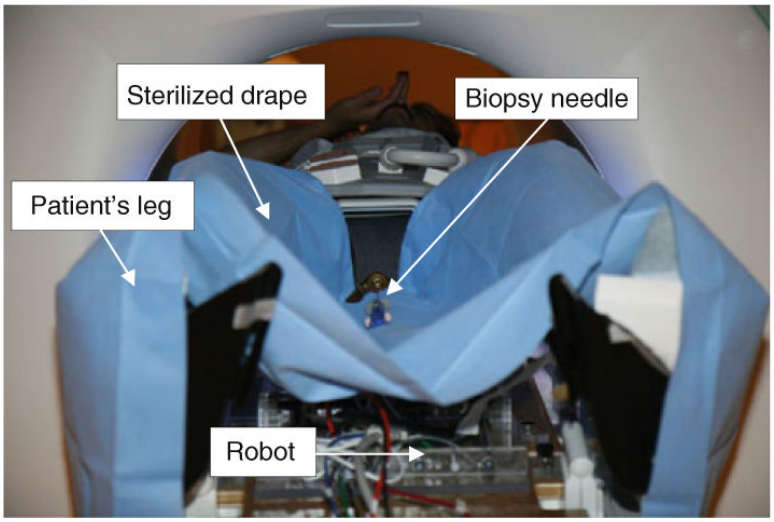

Fig. 5.
Robot is covered by a sterilized drape with a small hole on it for needle travel. Plasma sterilization is applied to top parts

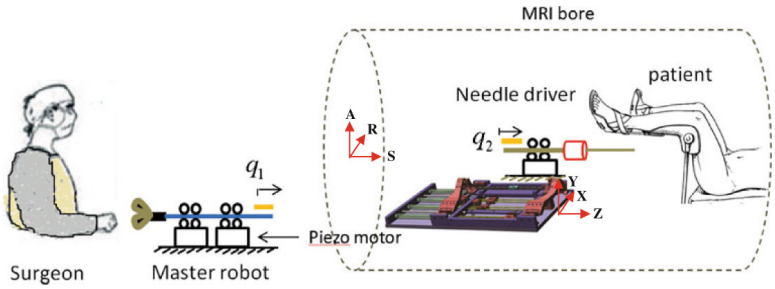

Fig. 6.

Schematic view of the overall master–slave system. The surgeon interacts with a master device to insert a needle at remote site. The surgeon is provided haptic and visual feedback

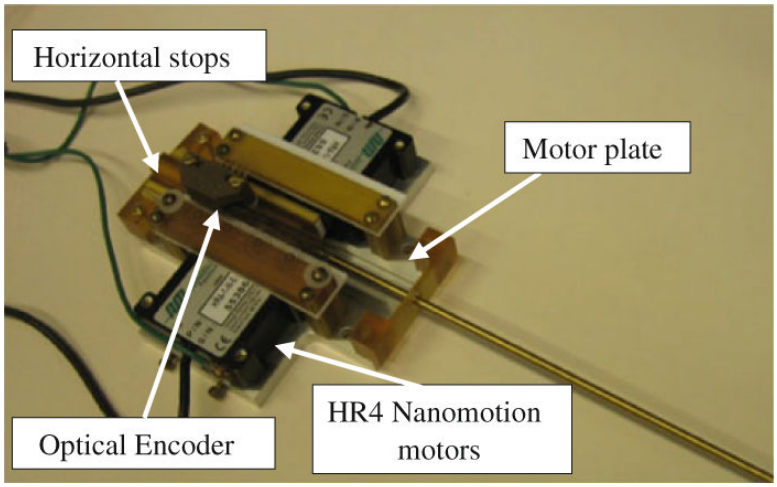

Fig. 7.
The needle driver: Two HR4 Nanomotion motors (28N together) are placed against each other. Optical encoder is employed for position feedback

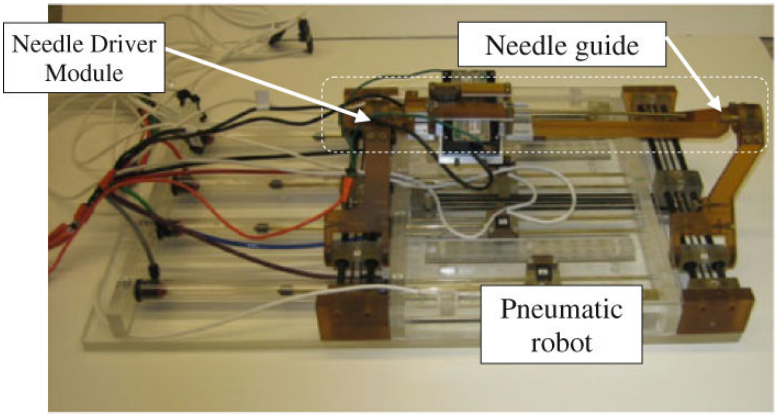

Fig. 8.
The needle driver is installed on top of the pneumatic robot. Dotted-line area shows sterilizable parts

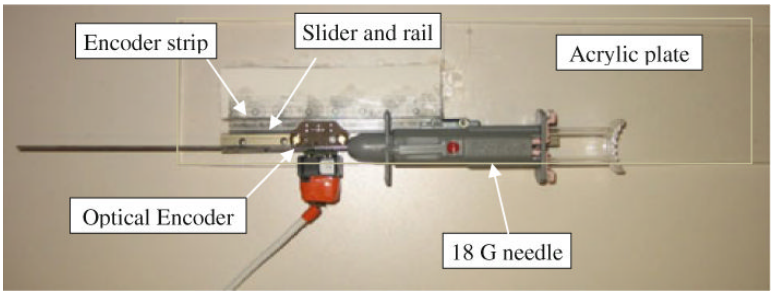

Fig. 9.
The master device: A needle is translated by a slider on a rail affixed to the Acrylic sheet. Position measurement is done by optical encoder

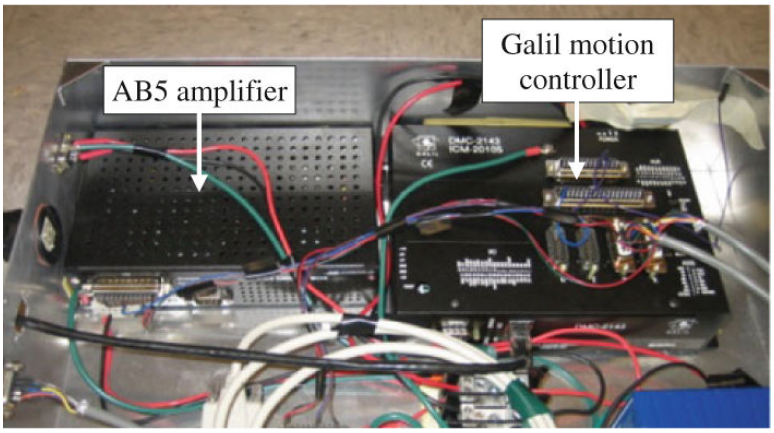

Fig. 10.
Galil motion controller and AB5 Nanomotion amplifier

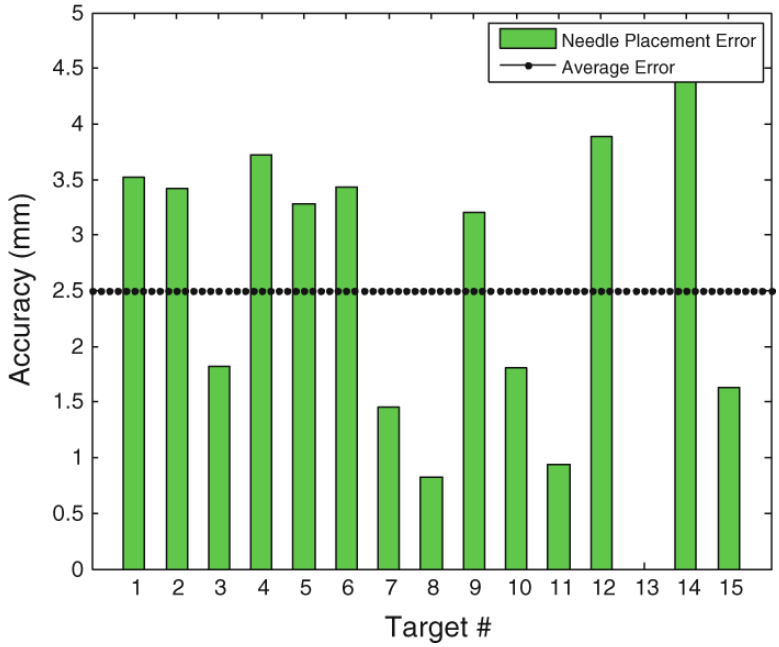

Fig. 11.
Overall needle placement error in ex vivo phantom experiment: the needle was bevel-tip 18G×20cm

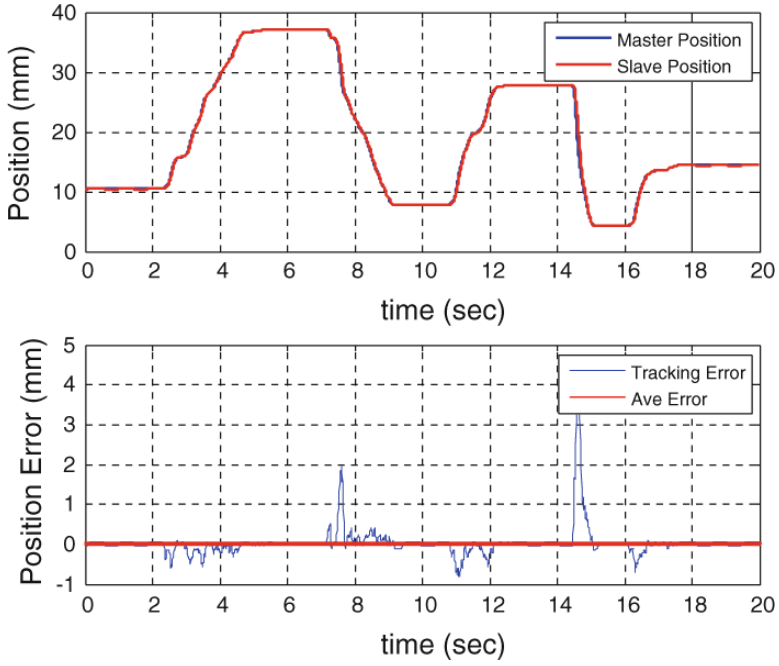

Fig. 12.
Position tracking of the master–slave needle insertion module

Table 1

Comparison of different piezo motors

Motor	MRI compatible	Max thrust (N)
Nanomotion	✓	Up to 32
PI	×	Not available
PiezoLEG	✓	10

Table 2

Results of needle placement accuracy evaluation in realistic phantom in 3T magnet (mm)

Target #	1	2	3	4	5	6	7	8	9	10	11	12	13	14	15	Avg	STD
R	9.0	20.4	9.6	15.3	2.1	2.4	9.6	15.60	11.1	15.0	11.0	13.0	0	2.4	9.6	–	–
A	16.3	15.8	28.3	21.5	15.8	24.0	10.9	11.50	12.0	17.0	22.0	18.0	0	24.0	10.9	–	–
S	12.5	12.5	12.5	22.0	22.0	22.0	32.0	32.00	12.5	12.5	12.5	20.0	0	25.0	25.0	–	–
Err_R	−1.3	2.1	0.3	3.7	2.6	0.5	−0.4	0.2	3.2	1.7	0.8	−1.2	0	3.5	−1.2	0.97	1.73
Err_A	3.2	2.7	−1.8	−0.4	2	3.4	1.4	0.8	0.1	−0.6	−0.5	3.7	0	3.1	1.1	1.22	1.74
Err_Total	3.5	3.4	1.8	3.7	3.2	3.4	1.4	0.8	3.2	1.8	0.9	3.8	0	4.6	1.6	2.50	1.37

Int J Comput Assist Radiol Surg. Author manuscript; available in PMC 2012 May 18.